Anal Bioanal Chem
DOI 10.1007/s00216-016-0147-z

RESEARCH PAPER

Nanostructured NiO-based reagentless biosensor for total cholesterol and low density lipoprotein detection

Gurpreet Kaur[1] · **Monika Tomar**[2] · **Vinay Gupta**[1]

Received: 19 September 2016 / Revised: 29 November 2016 / Accepted: 12 December 2016

Abstract Nanostructured nickel oxide (NiO) thin film has been explored as a matrix to develop a reagentless biosensor for free and total cholesterol as well as low density lipoprotein (LDL) detection. The redox property of the matrix has been exploited to enhance the electron transfer between the enzyme and the electrode as well as to eliminate the toxic mediator in solution. X-ray diffraction, scanning electron microscopy, atomic force microscopy, and Fourier transform infrared spectroscopy were carried out to characterize the NiO thin film. Biosensing response studies were accomplished using cyclic voltammetry (CV), electrochemical impedance spectroscopy (EIS), and differential pulse voltammetry (DPV). The developed biosensors exhibited a high sensitivity of 27 and 63 μA/mM/cm^2 over a linear range of 0.12–10.23 and 1–12 mM, respectively, for free and total cholesterol. Reagentless estimation of LDL was also achieved over the wide range 0.018–0.5 μM with a sensitivity of 0.12 mA/μM/cm^2. The results are extremely promising for the realization of an integrated biosensor for complete detection of cholesterol in the serum samples.

Keywords Nickel oxide · Low density lipoprotein · Cholesterol · Reagentless biosensor

Electronic supplementary material The online version of this article (doi:10.1007/s00216-016-0147-z) contains supplementary material, which is available to authorized users.

✉ Vinay Gupta
drguptavinay@gmail.com

[1] Department of Physics and Astrophysics, University of Delhi, Delhi 110007, India

[2] Physics Department, Miranda House, University of Delhi, Delhi 110007, India

Introduction

Cholesterol is a vital component of cell membranes and acts as a precursor for hormones, apart from having several biological functions [1]. It is a sterol molecule which is transported in the blood through lipoproteins. Low density lipoprotein (LDL) is the main carrier of cholesterol which consists of cholesterol molecules in free (30%) as well as esterified form (70%) [2]. It is a large protein made up of cholesteryl esters, free unesterified cholesterol, triglycerides, and a protein molecule, apolipoprotein B-100. A higher concentration of cholesterol in the blood is related to various heart diseases and other disorders such as hypertension, arteriosclerosis, myocardial infarction, and cerebral thrombosis [3, 4]. Hence, the measurement of cholesterol levels is crucial and an integral part of clinical diagnosis.

The complete quantification of cholesterol in the blood requires the estimation of free cholesterol and total cholesterol as well as LDL. The existing diagnostic techniques include spectrophotometric assay and high performance liquid chromatography (HPLC) [5, 6]. Besides, LDL is usually quantified indirectly using the Friedwald equation [7, 8]. However, these methods lack sensitivity and specificity and are time consuming. Moreover, they are costly and require pretreatment of samples. Therefore, a simple, accurate, fast, and low cost method capable of complete cholesterol determination is highly desirable [9]. In this context, electrochemical biosensors propose an attractive alternative because of their sensitivity, low detection limits, and rapid response. Electrochemical biosensors can be miniaturized into portable handheld devices for point of care diagnostics [10]. Majority of electrochemical biosensors demand the addition of some external mediator (such as potassium ferricyanide) in solution for transfer of electrons which are toxic and hinder the realization of integrated and implantable devices [11]. There are few reports on reagentless biosensors, including those for cholesterol detection, where the mediator has been co-

Published online: 11 January 2017

immobilized along with the enzyme on the electrode [12–14]. But these sensors suffer from a major issue of leaching out of the mediator from electrode surface leading to stability issues. Zhang et al. developed a reagentless H_2O_2 biosensor by co-immobilizing methylene blue mediator along with the enzyme. However, it had a comparatively poor shelf life of 8 weeks [12]. The reagentless biosensor developed by Gao et al. for glucose with a redox polymer electrodeposited on the electrode also exhibited a poor shelf life of 4 weeks [13]. Vidal et al. demonstrated a reagentless cholesterol biosensor with a similar poor shelf life and low sensitivity of 2.5 μA/mM [14]. Hence, significant efforts are needed to improve the electrode design by incorporating the redox property in the matrix itself so that reagentless biosensor could be realized with improved stability.

Matrix is the heart of a biosensor and the key step in development of a biosensor is the immobilization of the biorecognition molecule on to the matrix [15]. In order to eliminate the mediator in solution, either the matrix should be capable of direct electron transfer from the redox center of enzyme to the electrode or possess a redox couple that can shuttle the electrons efficiently [16]. Nanostructured nickel oxide (NiO) thin film is an ideal choice for electrochemical biosensors owing to its high isoelectric point, biocompatibility, chemical stability, and rapid electron communication feature [17]. Further, NiO possesses a redox couple of its own (Ni(III)/Ni(II)) thus paving the way towards realizing a reagentless biosensor which is preferable for practical use [18]. The presence of mediating species inside the matrix itself will not only eliminate the hindrance caused by leaching of mediator but also improve the performance of the biosensor by increasing the electron transfer between the enzyme and the electrode.

The present work is an effort to develop a reagentless biosensor for estimation of free and total cholesterol as well as LDL using nanostructured NiO thin film deposited via chemical route. A good quality and reproducible thin film, where the particles are in nanostructured form, has been deposited on ITO-coated corning glass substrates using spin coating of the precursor solution. Enzymes cholesterol oxidase, cholesterol esterase, and antibody apolipoprotein B-100 (AAB) were employed as biorecognition elements for free cholesterol, total cholesterol, and LDL respectively. Biosensing response characteristics were studied using cyclic voltammetry (CV), differential pulse voltammetry (DPV), and electrochemical impedance spectroscopy (EIS).

Experimental

Materials and solutions

Cholesterol oxidase (ChOx) from streptomyces species has been procured from SRL Pvt. Ltd., India. LDL lyophilized powder and anti-LDL (AAB) monoclonal antibody were acquired from Calbiochem (Merck Millipore). Cholesterol esterase (ChEt) from *Pseudomonas* species, Triton X-100, polyoxyethylene-9-lauryl ether, *N*-hydroxisuccinimide (NHS), *N*-(3-dimethylaminopropyl)-*N*′-ethylcarbodiimide) (EDC), free cholesterol, and nickel acetate tetrahydrate ($Ni(OAc)_2{\cdot}4H_2O$) were procured from Sigma-Aldrich, USA. The chemicals were utilized without any further purification.

ChOx, ChEt, and AAB solutions (1 mg/ml) were prepared in 50 mM phosphate buffer saline (PBS) of pH 7.0 containing 0.9% NaCl. The stock solution of free cholesterol was made using 10% Triton X-100 and stored at 4 °C. Stock solution of cholesteryl oleate was prepared in polyoxyethylene-9-lauryl ether. Total cholesterol consists of 30% free cholesterol and 70% cholesterol oleate. For preparation of stock solution of LDL, the LDL powder was dissolved in de-ionized (DI) water containing 50 mM NaCl and 0.01% ethylene diamine tetra acetic acid (EDTA).

Preparation of bioelectrodes

For the preparation of nanostructured NiO thin film, 0.5 M $Ni(OAc)_2{\cdot}4H_2O$ was dissolved in DI water. A separate solution was prepared by dissolving 0.5 M NaOH in de-ionized water containing PVP keeping the ratio of NaOH:PVP as 3:1. PVP was added as a surfactant to prevent aggregation of the particles. The second solution was added dropwise to the first solution. The resulting dispersion was spin coated on an ITO (indium-doped tin oxide)-coated corning glass substrate of area 2 cm × 1 cm of which 1 cm × 1 cm area was masked for electrical contacts. This deposition was repeated six times and the films were dried at 150 °C after each coat. Finally, the films were annealed in air at 300 °C for 2 h to obtain pure and crystalline NiO structure.

ChOx, ChOx-ChEt, and LDL were covalently immobilized on three separate NiO thin films via EDC-NHS chemistry. The films were subjected to hydrolysis and silanization to activate the surface for covalent bonding as reported previously [19]. Twenty microliters of ChOx solution having 0.4 M EDC and 0.1 M NHS was then spread on one of the films and incubated for 2 h at 27 °C proceeded by rinsing with DI water to remove unbound enzyme molecules present on the surface of the bioelectrode (ChOx/NiO/ITO/glass). The bioelectrode was stored at 4 °C when not in use. Similarly, 20 μl each of ChOx-ChEt and AAB solutions were immobilized on other NiO films using the same protocol to obtain the respective bioelectrodes (ChEt-ChOx/NiO/ITO/glass and AAB/NiO/ITO/glass). For total cholesterol estimation, ChOx and ChEt (10 μl each) were co-immobilized on the surface of NiO thin film.

Measurements and apparatus

Characterization of the prepared NiO thin film was carried out by X-ray diffraction (XRD, Bruker D8 Discover), Fourier

transform infrared (FTIR, Perkin Elmer Frontier) spectroscopy, and scanning electron microscopy (SEM, Tescan MIRA3). All electrochemical measurements were performed on Gamry Reference 600 Potentiostat/Galvanostat by means of a three-electrode cell configuration in PBS (pH 7.0) utilizing Ag/AgCl as the reference electrode and platinum as the counter electrode. All measurements were taken in the absence of any artificial mediator except for the EIS measurements where $[Fe(CN)_6]^{3-/4-}$ was added in to PBS.

Results and discussion

Structural and morphological characterization

The XRD pattern of the deposited NiO thin film, as shown in Fig. 1, shows characteristic peaks at 36.8°, 43.1°, and 62.8° related to (111), (200), and (220) planes of cubic NiO [20]. The crystallite size was determined from the Scherrer equation and was found to be 5 nm for the crystallites oriented along the (200) plane. The lattice parameter was evaluated to be $a = 4.212$ Å which is larger as compared to the bulk value (4.177 Å) indicating the existence of tensile stress in the NiO thin film leading to expansion of the unit cell [21]. Thus, XRD studies indicate the growth of polycrystalline NiO thin films having nanosized crystallites.

Figure 2a–d depicts the SEM images of NiO thin film deposited over ITO/glass electrode, ChOx/NiO/ITO/glass, ChEt-ChOx/NiO/ITO/glass, and AAB/NiO/ITO/glass bioelectrodes, respectively. Presence of spherical-shaped nanostructures can be seen from the SEM image of NiO thin film. Highly porous structure consisting of nanosized grains (30–40 nm) was observed in the film which is advantageous for successful loading of various biomolecules [22]. Upon immobilization of enzymes ChOx and ChOx-ChEt, large globular structures were seen on the surface of NiO thin films (Fig. 2b, c). Large Y-shaped structures were observed on the AAB/NiO/ITO/glass bioelectrode confirming the immobilization of the antibody on NiO thin film. For more clarity, the images at higher magnification are also included (see Electronic Supplementary Material (ESM) Fig. S1(a to d)). Nanograins in NiO are clearly visible in the image at lower scale. For the bioelectrodes, similar morphology can be observed from the SEM images at higher magnification. Surface morphology and modification has also been studied using AFM measurements (ESM Fig. S2(a to d)). Stetsyshyn et al. have also utilized AFM measurements to study the variation in surface morphology of poly(ethylene terephthalate) before and after modification by oligoperoxides and dextran [23]. A distinct change in the topography can be seen for NiO thin film after modification by biomolecules. Significant increase in height and roughness is also observed with immobilization of biomolecules.

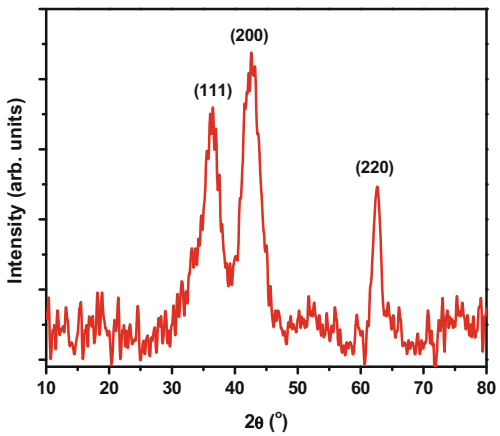

Fig. 1 XRD spectra of the nanostructured NiO thin film

FTIR studies

The optical characterization of the films before and after immobilization of biomolecules was carried out using FTIR spectroscopy and the corresponding spectra are shown in Fig. 3a–d. NiO thin film exhibits bands at 435, 521, and 648 cm^{-1} corresponding to the stretching vibration modes of Ni–O and Ni–O–Ni bond (Fig. 3a) [24]. After immobilization of enzyme ChOx, additional bands were observed at 864 and 1010 cm^{-1} that are associated with stretching vibrations of C–N amine linkages and C–O stretching of amide band of the enzyme confirming the immobilization of the enzyme (Fig. 3b) [25]. Further bands were seen at 1420, 1569, and 1640 cm^{-1} related to C–N axial deformation and carbonyl stretch of amide II and N–H bending of amide I band [26]. Similar absorption bands were observed after co-immobilization of ChOx-ChEt enzymes at 863, 1006, 1411, 1564, and 1652 cm^{-1} which validate the presence of enzyme on the NiO thin film (Fig. 3c). Figure 3d illustrates the FTIR spectrum of the film upon immobilization of the antibody. Additional bands characteristic of the proteins were observed at 852, 1009, 1560, and 1649 cm^{-1} analogous to the enzyme-based bioelectrodes [27]. Another band at 1289 cm^{-1} related to the amide III linkages was also seen. The existence of these bands reveals the successful binding of the antibody on the NiO film. A broad band at around 3450 cm^{-1} was observed in all the bioelectrodes which may be due to the presence of water molecules (O–H bond) or due to amide B band of the biomolecules. FTIR studies clearly confirm the immobilization of enzymes on the NiO thin film surface.

Cyclic voltammetry studies

Figure 4 shows the cyclic voltammograms of bare ITO-coated corning glass electrode, NiO/ITO/glass, ChOx/NiO/ITO/glass, ChEt-ChOx/NiO/ITO/glass, and AAB/NiO/ITO/glass bioelectrodes in PBS solution without any external mediator

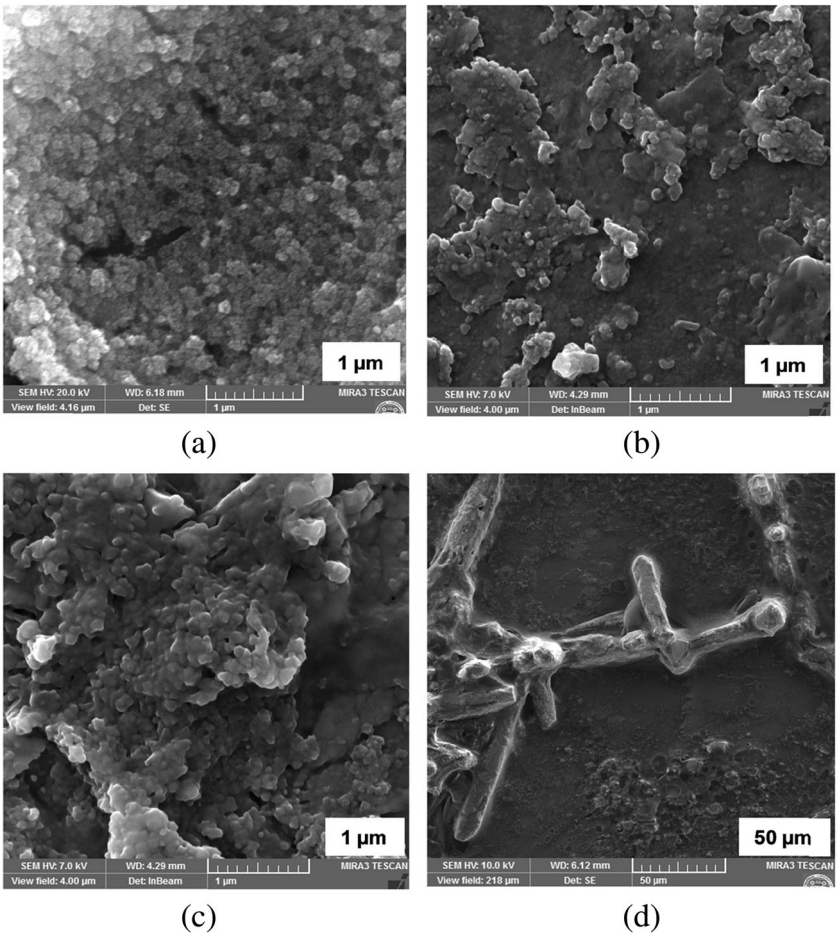

Fig. 2 SEM images of the **a** nanostructured NiO thin film, **b** ChOx/NiO/ITO/glass bioelectrode, **c** ChEt-ChOx/NiO/ITO/glass bioelectrode, and **d** AAB/NiO/ITO/glass bioelectrode

in solution in the voltage range −0.3 to +0.8 V. Bare ITO does not give a CV curve in the absence of mediator as it lacks a redox couple of its own. However, NiO thin film deposited over ITO exhibits proper CV curve with well defined oxidation and reduction peaks. These peaks correspond to the reduction and oxidation potential of Ni(III) and Ni(II) present in NiO. The redox peaks are due to the reversible reaction of Ni(III)/Ni(II) states of NiO/NiOOH which can be illustrated by the following reaction:

$$NiO + OH^{-} - e^{-} \rightarrow NiOOH$$

Thus, the matrix employed in this case (NiO) itself shows redox activity and eliminates the need of any external mediator in solution [18].

Upon immobilization of the enzyme ChOx on NiO thin film, the peak oxidation current decreased drastically from 695 to 420 μA. This may be attributed to the insulating nature of the bulky enzyme molecules. The ChEt-ChOx/NiO/ITO/glass bioelectrode also showed similar behavior with a reduction in the value of peak oxidation current to 315 μA. The AAB/NiO/ITO/glass bioelectrode showed further decrease in current to 260 μA following immobilization of the antibody. The presence of large antibody molecules on the film obstructs the flow of current leading to a considerable decrease in the peak oxidation current.

The scan rate variation studies were carried out for all the three bioelectrodes in order to determine the charge transfer process involved in the electrochemical reactions as well as to estimate the concentration of ionic species on the surface of the respective bioelectrodes. All the three bioelectrodes displayed similar behavior with variation in scan rate from 80 to 170 mV/s and the corresponding CV curves are shown in Fig. 5a–c. With an increase in scan rate, the oxidation potential was found to shift to higher value whereas the reduction potential shifts towards lower potential proposing a quasi-reversible process [28]. The peak oxidation (I_{po}) and reduction currents (I_{pr}) were found to be proportional to the scan rate indicative of a surface controlled process (inset: Fig. 5a–c).

The surface concentration of the ionic species (Γ) on the surface of the bioelectrode was evaluated by employing the following equation-

$$I_{po} = \frac{F^2 \Gamma A v}{4RT}$$

where, F is the Faraday constant, v is the scan rate, R is the gas constant, T is the temperature, and A is the area of the electrode in

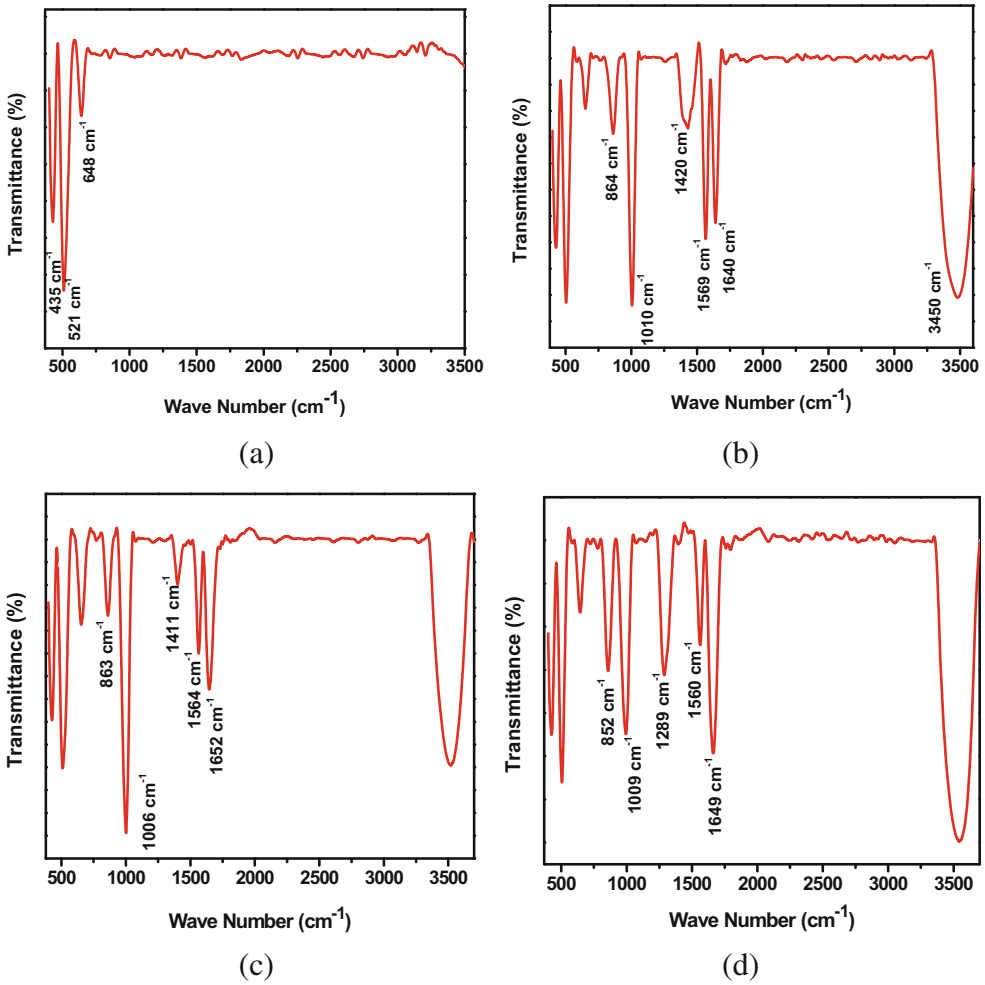

Fig. 3 FTIR spectra of **a** NiO thin film, **b** ChOx immobilized NiO thin film, **c** ChEt-ChOx immobilized NiO thin film, and **d** AAB immobilized NiO thin film

square centimeter [29]. As per 2014 IUPAC Recommendation [30], it is difficult to directly extract the number n of electrons involved in the rate-determining step from the true transfer coefficient, without making some arbitrary hypothesis on the electrode reaction mechanism. In view of this, n is removed (i.e., replaced by unity) from the equations. The value of I_{po}/v can be computed from the slope of the plot of peak oxidation current and scan rate. The value of Γ was found to be 2.6×10^{-7} mol cm^{-2} for ChOx/NiO/ITO/glass bioelectrode which is higher than the corresponding values previously reported [31]. ChEt-ChOx/NiO/ITO/glass bioelectrode showed a value of $\Gamma = 2.8 \times 10^{-7}$ mol cm^{-2} implying enhanced loading of enzyme molecules on the surface of nanostructured NiO thin film. A higher value of Γ was estimated (5.4×10^{-7} mol cm^{-2}) for AAB/NiO/ITO/glass bioelectrode which may be attributed to efficient loading of antibody molecules. The heterogeneous electron transfer rate constant (k_s) of the bioelectrodes can be determined using the Laviron equation

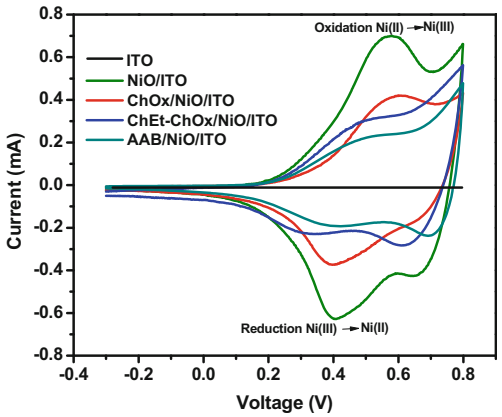

Fig. 4 CV curves of bare ITO/glass, NiO/ITO/glass, ChOx/NiO/ITO/glass, ChEt-ChOx/NiO/ITO/glass, and AAB/NiO/ITO/glass bioelectrodes obtained without any external mediator in the PBS solution

$$\log k_s = \alpha\log(1-\alpha) + (1-\alpha)\log\alpha - log\frac{RT}{F\nu} - \frac{\alpha(1-\alpha)F\Delta E_p}{2.3\,RT}$$

where ΔE_p is the peak to peak separation at a scan rate of ν and other symbols have their usual meanings [32]. The charge transfer coefficient α can be calculated from the slope of the graph between oxidation peak potential and log of scan rate using the relation

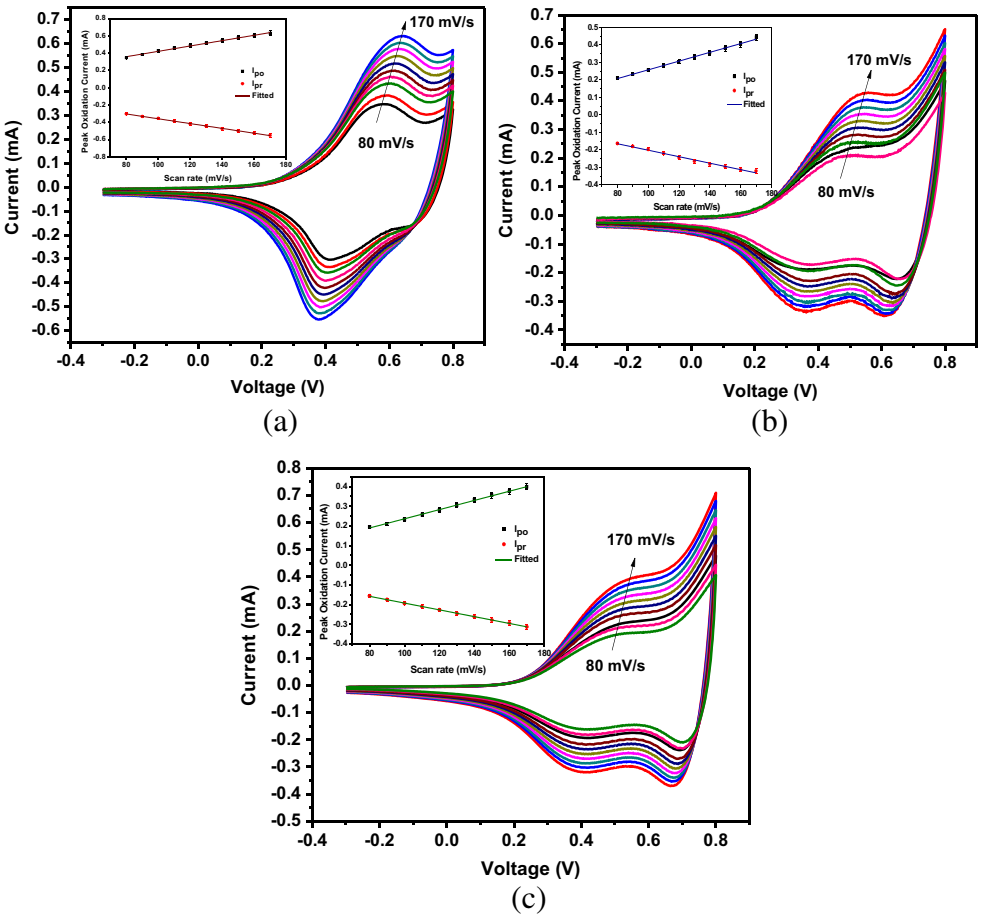

Fig. 5 Scan rate variation for the **a** ChOx/NiO/ITO/glass, **b** ChEt-ChOx/NiO/ITO/glass, and **c** AAB/NiO/ITO/glass bioelectrodes (*inset*: the variation of peak oxidation (I_{po}) and reduction currents (I_{pr}) as a function of square root of scan rate for the respective bioelectrodes

$$\text{Slope} = \frac{2.3RT}{(1-\alpha)F}$$

Taking the value of $\alpha = 0.67$, the value of k_s was found to be 3.45 s^{-1} for the ChOx/NiO/ITO/glass bioelectrode which is much larger as compared to other reports implying a fast electron transfer which may be an attribute of the nanostructured NiO matrix [33]. The NiO nanostructures in the bioelectrode act as good acceptors of the electrons generated during oxidation of the enzyme, which are transferred to the underneath ITO electrode, resulting in higher electron transfer rate constant. Further, the nanostructures provide high surface-to-volume ratio for immobilization of biomolecules. The electrons are transferred efficiently through the defects present in the semiconducting NiO matrix thereby giving enhanced electron transfer. Similarly, the corresponding values for ChEt-ChOx/NiO/ITO/glass and AAB/NiO/ITO/glass bioelectrodes were computed to be 3.9 and 1.65 s^{-1}, respectively. The lower value in case of AAB/NiO/ITO/glass bioelectrode may be due to the presence of large-sized antibody molecules due to which shuttling of electrons may not be as efficient as in case of the other two bioelectrodes.

Biosensing response characteristics

The biosensing response studies for free and total cholesterol were carried out using cyclic voltammetry. Figure 6a illustrates the CV curves obtained for the ChOx/NiO/ITO/glass bioelectrode with varying concentrations of free cholesterol in the solution. The peak oxidation current was observed to increase continuously with consecutive addition of cholesterol ranging from 0.12 to 10.23 mM (Fig. 6a). The detection mechanism can be explained as follows: ChOx immobilized on the NiO film oxidizes the free cholesterol into cholestenone and in the process itself gets reduced. In order to get re-oxidized, ChOx loses an electron to Ni present in the NiO matrix in the Ni(III) state converting it into Ni(II), which transfers the electron to the electrode returning to the Ni(III) state. With increase in concentration of cholesterol, more number of electrons are generated as a result of increased oxidation leading to higher peak oxidation current. The opposite process proceeds in the reverse voltage scan. Inset of Fig. 6a shows the calibration curve depicting a linear increase in the peak oxidation current with increasing concentration of cholesterol which is due to the loss and gain of electrons in the biochemical reaction via NiO matrix. The sensitivity of the biosensor towards free cholesterol, as computed from the calibration curve, was found to be 27 μA/mM/cm^2.

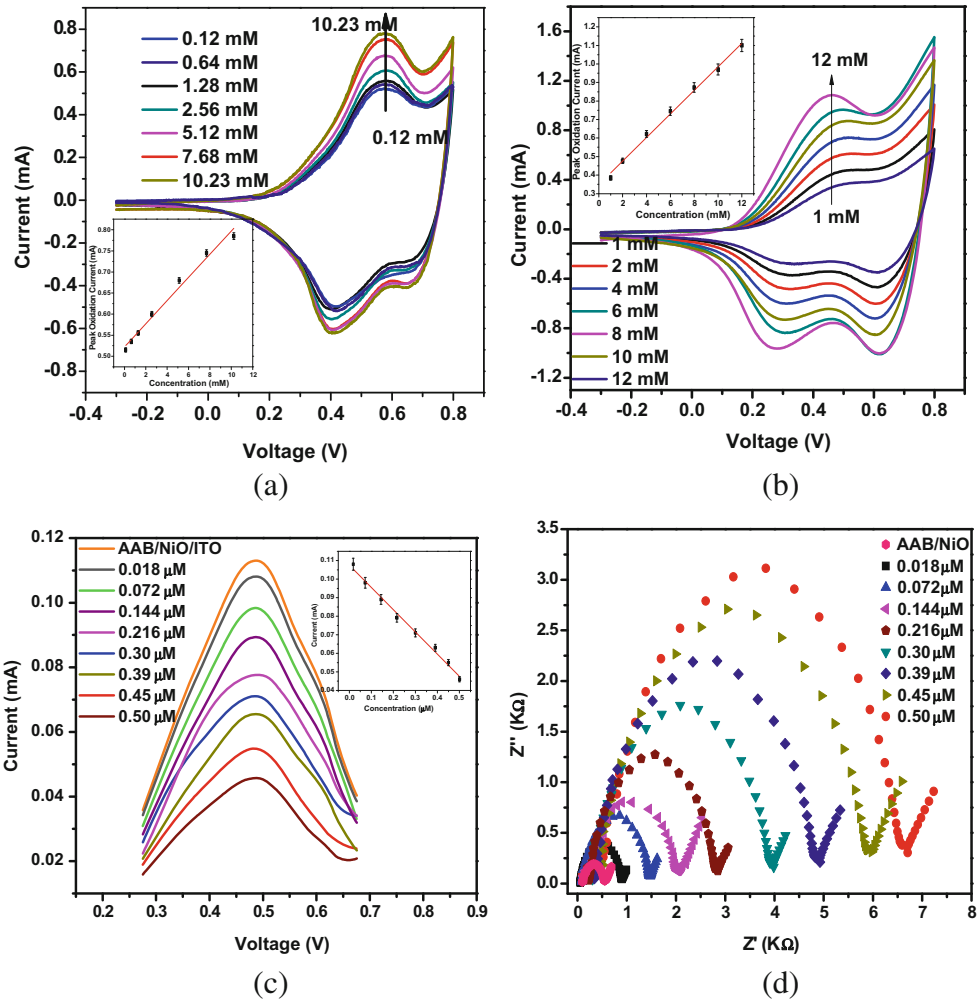

Fig. 6 Biosensing response studies (CV) of **a** ChOx/NiO/ITO/glass bioelectrode and **b** ChEt-ChOx/NiO/ITO/glass bioelectrode. **c** DPV and **d** EIS spectra of the AAB/NiO/ITO/glass bioelectrode with LDL concentration (*insets* show the corresponding calibration plots)

The high value of sensitivity even in the absence of any external mediator can be accredited to the swift electron communication feature of prepared nanostructured NiO thin film [34]. The biosensor exhibited a fast response time of 5 s.

Similarly, for total cholesterol estimation, CV curves were recorded with different concentrations of total cholesterol in the PBS solution (Fig. 6b). The value of peak oxidation current increases linearly with increase in concentration of total cholesterol from 1 to 12 mM (physiological range: 3.1–6.5 mM). The sensing mechanism for total cholesterol is analogous to that of free cholesterol except that two enzymes (ChOx and ChEt) are involved in this case. Total cholesterol consists of both free cholesterol and cholesterol esters (cholesterol oleate). ChEt enzyme transforms the cholesterol esters into free cholesterol and then ChOx catalyzes the oxidation of free cholesterol and the process continues in the same way as in the case of free cholesterol estimation. The sensitivity in this case was evaluated to be 63 μA/mM/cm^2 (Inset: Fig. 6b). The sensing mechanism for both free and total cholesterol has been depicted using a schematic in ESM Fig. S3. Majority of reports on cholesterol biosensors have utilized some external mediator (generally, potassium ferricyanide) and hence, the present work offers additional advantage apart from the high value of sensitivity which is higher than the corresponding values reported in literature [34, 35].

In case of LDL, the change in current in CV for various concentrations was not appreciable. Hence, electrochemical impedance spectroscopy (EIS) and differential pulse voltammetry (DPV) were exploited for the biosensing response studies. The results obtained by the DPV measurements carried out for the AAB/NiO/ITO/glass bioelectrode in PBS devoid of any external artificial mediator are shown in Fig. 6c. The bioelectrode was incubated with different concentrations of LDL for 3 h in a humid chamber before taking DPV and EIS measurements. The DPV curve of the AAB/NiO/ITO/glass bioelectrode which shows a well defined oxidation peak at around 0.49 V is observed exhibiting a current of 0.11 mA. This oxidation peak is due to the oxidation of the Ni(II) state of the NiO matrix into Ni(III) state. This is a single electron transfer process between the two oxidation states of Ni in NiO matrix. Upon incubation with LDL, the current decreases due to the insulating nature of the antibody-antigen immunocomplex. However, there is no significant shift

in the peak voltage which is related to the oxidation of Ni(II). The peak oxidation current decreased continuously with increase in LDL concentration. The observed decrease is a consequence of formation of large insulating antibody-antigen immunocomplex which prevents the electron transfer to the external circuit. Inset of Fig. 6c shows the calibration curve depicting a linear decrease in oxidation current over a concentration of LDL ranging from 0.018 to 0.5 μM with a sensitivity of 0.12 mA/μM/cm^2 (physiological range 0.144–0.30 μM). Figure 6d represents the Nyquits plots (EIS curves) of the AAB/NiO/ITO/glass bioelectrode in the frequency range 0.01–10^5 Hz. These measurements were, however, performed in the presence of $[Fe(CN)_6]^{3-/4-}$ as mediating species (5 mM in PBS). Typical semicircle behavior in EIS is observed in all the cases where diameter of the semicircle signifies the charge transfer resistance (R_{CT}) offered by the electrodes. The semicircle part, observed at higher frequencies, is associated with the electron transfer limited process, while the linear part seen at lower frequencies is characteristic of a diffusion limited process. The EIS data has been modeled using equivalent electrolyte resistance (R_S), in series with a parallel combination of capacitance of the dielectric layer (C_{DL}) with a series combination of charge-transfer resistance (R_{CT}) and Warburg impedance (Z_W). The value of R_{CT} is related to the hindrance to the current flow produced by redox reactions at the interface of prepared electrodes with PBS and was found to increase to 554 kΩ when antibody was immobilized over the NiO thin film. These results are consistent with the CV measurements. After incubation with LDL, the value of R_{CT} further increased owing to the creation of the antibody-antigen immunocomplex and due to the charge hindrance generated by the protein molecules. R_{CT} showed a linear increase with increase in concentration of LDL from 0.018 to 0.5 μM. The observed increase in R_{CT} value is attributed to the increase in accumulation of antigen-antibody immunocomplex on the surface of AAB/NiO/ITO immunoelectrode which functions as a barrier for charge communication. Moreover, LDL is negatively charged at pH 7.0 and offers electrostatic force of repulsion to the electrons transferring from negative redox couple $[Fe(CN)_6]^{3-/4-}$, thereby resulting in an increase in the R_{CT} value.

In order to investigate the enzyme kinetics, the Michaelis-Menten constant (K_m) was calculated for both the enzyme-based bioelectrodes. ESM Fig. S4(a) and (b) shows the Hanes plots of ChOx/NiO/ITO/glass and ChEt-ChOx/NiO/ITO/glass bioelectrodes, respectively. The K_m value was obtained to be 0.47 mM for ChOx and 1.9 mM for ChEt-ChOx. A lower value of K_m suggests higher affinity of the enzyme towards its substrate highlighting the effective immobilization of the enzymes on the NiO matrix [36].

For the AAB/NiO/ITO/glass bioelectrode, the surface coverage of the LDL molecules was calculated using the expression

$$\Theta = 1 - \frac{R_o}{R_i}$$

where R_o is the charge transfer resistance of AAB/NiO/ITO/glass bioelectrode and R_i is the charge transfer resistance of the bioelectrode after incubation with a specific concentration of LDL. Θ gives a measure of the binding sites of the antibody which are occupied by the antigen [37]. The values of Θ were estimated for different concentrations of LDL and the corresponding curve is shown in ESM Fig. S4(c). It can be observed that it increases with the increase in the concentration of LDL and tends to saturate at higher values implying that at higher concentrations, higher number of molecules bind to the antibodies at the binding sites available. All the electrochemical measurements throughout the study were repeated ten times and the observations are within ±3% error. This shows repeatability of the results over the same bioelectrode.

Table 1 Comparison of the response characteristics of the present biosensor with previous reports in literature

Analyte	Matrix	Sensitivity	Linear range	Limit of detection	Shelf life	Reagentless	Reference
Free cholesterol Total cholesterol	ATP SAM	542.3 nA mM^{-1}, 886.6 nA mM^{-1}	0.6–10.3 mM	–	16 weeks	Yes	[33]
Total cholesterol	Au nanowire	0.85 μA mM^{-1}	0.01–0.06 μM	–	10 days	No	[25]
Total cholesterol	MWCNT-chitosan	0.2 μA mM^{-1}	0.5–5 mM	–	20 days	No	[38]
Total cholesterol	MWCNT-SiO_2-chitosan	3.8 μA mM^{-1}	2.5–12.93 mM	–	10 weeks	No	[39]
Free cholesterol	Fe_3O_4	2.15 μA mM^{-1} cm^{-2}	0.25–12.5 mM	0.92 mM	9 weeks	Yes	[40]
Free cholesterol	$NiFe_2O_4$-CuO-FeO	21.5 μA mM^{-1} cm^{-2}	0.12–12.93 mM	0.8 mM	12 weeks	No	[41]
Free cholesterol	ZnO nanoparticles-chitosan	2.28 μA mM^{-1}	Up to 7.75 mM	0.12 mM	8 weeks	No	[31]
LDL	Chitosan-CNT	31 Ω μM^{-1} cm^{-2}	Up to 0.36 μM	0.03 μM	7 weeks	–	[42]
LDL	Polyaniline	11.25 k Ω μM^{-1}	0.018–0.39 μM	–	–	–	[43]
Free cholesterol Total cholesterol LDL	NiO	27 μA mM^{-1} cm^{-2} 63 μA mM^{-1} cm^{-2} 0.12 mA μM^{-1} cm^{-2}	0.12–10.23 mM 1–12 mM 0.018-0.5 μM	0.1 mM 0.5 mM 0.015 μM	18 weeks	Yes	Present work

Table 2 Real sample analysis of ChEt-ChOx/NiO/ITO/glass bioelectrode

Sample number	Total cholesterol concentration (mM)		R.S.D. of developed biosensor ($n = 3$)	Spike (mM)	Data after spike		
	Biosensor	Spectrophotometric			Cholesterol concentration (mM)	Recovery (%)	R.S.D. of developed biosensor ($n = 3$)
1	3.81	3.86	1.8%	2	5.82	98.1	1.7%
2	4.68	4.63	2.1%	2	6.68	101	2.2%

Table 1 compares the present work with some of the previous reports on cholesterol biosensors. The main advantage of the present work is the absence of any external redox mediator. There are very few reports on the realization of a reagentless biosensor for cholesterol. As compared to those reported, the present results exhibit high sensitivity and low limit of detection. Also, the same matrix has been fabricated in triplicate and utilized for the detection of free cholesterol, total cholesterol, and LDL. Due to the high stability and biocompatibility of the nanostructured film, the shelf life of these biosensors is found to be much longer than previous reports. The linear range and limit of detection of the present biosensor are better or comparable to those reported previously. In case of LDL, there are very few reports on electrochemical biosensors specially those that are label free. Moreover, NiO in the form of nanostructures provides high surface-to-volume ratio and strong adsorption ability which further aids in biosensing applications.

Reproducibility, validation, stability, and selectivity of the biosensor

Each bioelectrode was fabricated in triplicate and tested for a fixed concentration of free cholesterol, total cholesterol, and LDL (2.56 mM, 4 mM, and 0.216 μM, respectively) using CV and DPV, and the value of peak oxidation current was found to be almost same with a relative standard deviation (RSD) of 1.06, 1.18, and 1.30%, respectively (ESM Fig. S5(a to c)). To validate the fabricated biosensor, its testing was done in two real human serum samples. However, it is important to note that cholesterol is found in blood in the free form (about 30% of the total content) or as cholesterol esters (approximately 70% of the total content). The laboratory value of free cholesterol is generally not available, and hence, only total cholesterol bioelectrode was tested. The results indicate that the cholesterol concentration in serum

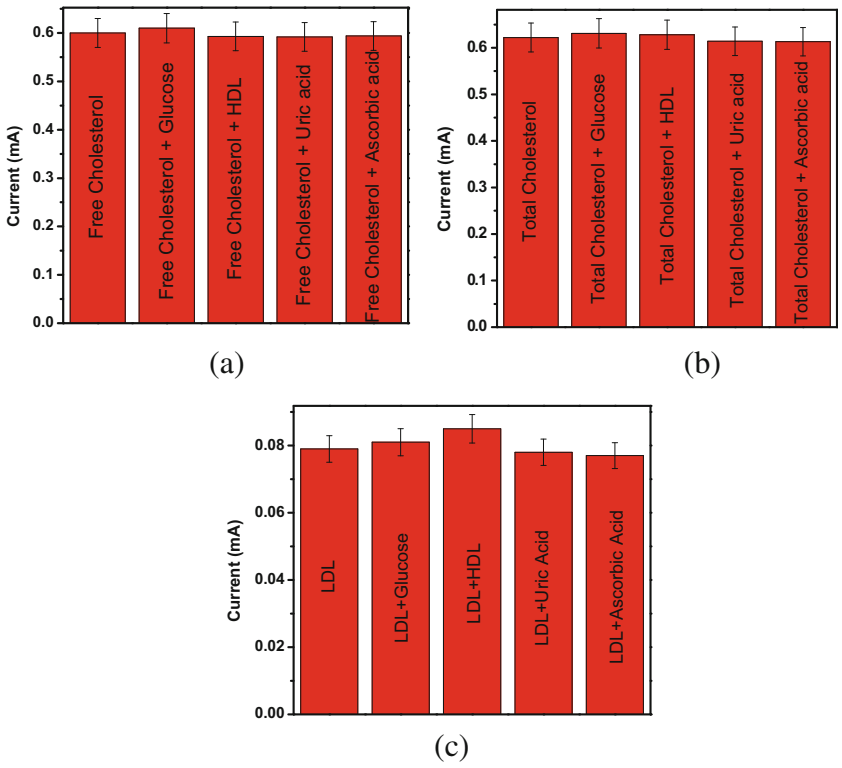

Fig. 7 Interference studies for **a** ChOx/NiO/ITO/glass, **b** ChEt-ChOx/NiO/ITO/glass, and **c** AAB/NiO/ITO/glass bioelectrodes in the presence of different analytes

determined using the developed biosensor agreed well with the spectrophotometric data obtained from the laboratory tests (Table 2). Real samples were then spiked with known concentration (2 mM) of cholesterol and the recovery tests for cholesterol were performed. The amounts of added cholesterol were then evaluated by using the fabricated biosensor. These results demonstrate that the developed biosensor is accurate and precise and its performance is comparable with the commercially accepted methods. The selectivity of the biosensors was examined by taking the sensing response after addition of normal concentrations of various interferents including glucose (5 mM), uric acid (0.1 mM), ascorbic acid (0.05 mM), and high density lipoprotein (30 mg/dl) in the buffer along with cholesterol (free, total, and LDL separately) (Fig. 7a–c). The maximum interference that was obtained was less than 3% which is well within the acceptable limits. Hence, the biosensors are highly specific towards cholesterol.

The stability of the fabricated biosensors was investigated by examining the current response for a specific concentration of analyte at regular intervals over a period of 18 weeks. ChOx/NiO/ITO/glass and ChEt-ChOx/NiO/ITO/glass bioelectrodes maintained 90% activity whereas the AAB/NiO/ITO/glass bioelectrode retained 88% activity even after 18 weeks demonstrating the long shelf life of the biosensors. The high shelf life of the biosensors can be ascribed to the extraordinary stability and biocompatibility of NiO matrix.

Conclusion

The results illustrate that the nanostructured NiO matrix is a promising candidate for application in reagentless biosensors. There is hardly any report in literature which demonstrates the complete detection of cholesterol (free, total, and LDL). Moreover, the presence of the mediating species in the matrix itself is highly beneficial. Consequently, the deposited NiO thin film is capable of detecting free cholesterol, total cholesterol, and LDL over a wide linear range with a high sensitivity and long shelf life.

Acknowledgements The authors are grateful to the Department of Science and Technology (DST), Ministry of Science and Technology for the financial support. GK gratefully acknowledges the University Grants Commission (UGC) for research fellowship.

Compliance with ethical standards

Conflict of interest The authors declare that they have no conflict of interest.

References

1. Vance JE and Vance DE. Biochemistry of lipids, lipoproteins and membranes. Elsevier; 1991.
2. Hevonoja T, Pentikäinen MO, Hyvönen MT, Kovanen PT, Ala-Korpela M. Structure of low density lipoprotein (LDL) particles: basis for understanding molecular changes in modified LDL. Biochim Biophys Acta Mol Cell Biol Lipids. 2000;1488:189.
3. Kannel WB, Castelli WP, Gordon T, Mcnamara PM. Serum cholesterol, lipoproteins, and the risk of coronary heart disease: the Framingham Study. Ann Intern Med. 1971;74:1.
4. Stampfer MJ, Sacks FM, Salvini S, Willett WC, Hennekens CH. A prospective study of cholesterol, apolipoproteins, and the risk of myocardial infarction. N Engl J Med. 1991;325:373.
5. Jurand J, Albert-Recht F. The estimation of serum cholesterol. Clin Chim Acta. 1962;7:522.
6. El-Saadani M, Esterbauer H, El-Sayed M, Goher M, Nassar AY, Jürgens G. A spectrophotometric assay for lipid peroxides in serum lipoproteins using a commercially available reagent. J Lipid Res. 1989;30:627.
7. Sahu S, Chawla R, Uppal B. Comparison of two methods of estimation of low density lipoprotein cholesterol, the direct versus Friedewald estimation. Indian J Clin Biochem. 2005;20:54.
8. Friedewald WT, Levy RI, Fredrickson DS. Estimation of the concentration of low-density lipoprotein cholesterol in plasma, without use of the preparative ultracentrifuge. Clin Chem. 1972;18:499.
9. Malhotra BD, Chaubey A. Biosensors for clinical diagnostics industry. Sensors Actuators B. 2003;91:117.
10. Wang J. Electrochemical biosensors: towards point-of-care cancer diagnostics. Biosens Bioelectron. 2006;21:1887.
11. Chaubey A, Malhotra BD. Mediated biosensors. Biosens Bioelectron. 2002;17:441.
12. Zhang Y, Liu L, Xi F, Wu T, Lin X. A simple layer-by-layer assembly strategy for a reagentless biosensor based on a nanocomposite of methylene blue-multiwalled carbon nanotubes. Electroanalaysis. 2010;22:277.
13. Gao Q, Guo Y, Zhang W, Qi H, Zhang C. An amperometric glucose biosensor based on layer-by-layer GOx-SWCNT conjugate/redox polymer multilayer on a screen-printed carbon electrode. Sensors Actuators B. 2011;153:219.
14. Vidal JC, Espuelas J, Castillo JR. Amperometric cholesterol biosensor based on in situ reconstituted cholesterol oxidase on an immobilized monolayer of flavin adenine dinucleotide cofactor. Anal Biochem. 2004;333:88.
15. Xu Z, Chen X, Dong S. Electrochemical biosensors based on advanced bioimmobilization matrices. TrAC Trends Anal Chem. 2006;25:899.
16. Jindal K, Tomar M, Gupta V. Inducing electrocatalytic functionality in ZnO thin film by N doping to realize a third generation uric acid biosensor. Biosens Bioelectron. 2014;55:57.
17. Li C, Liu Y, Li L, Du Z, Xu S, Zhang M, et al. A novel amperometric biosensor based on NiO hollow nanospheres for biosensing glucose. Talanta. 2008;77:455.
18. Tyagi M, Tomar M, Gupta V. Glad assisted synthesis of NiO nanorods for realization of enzymatic reagentless urea biosensor. Biosens Bioelectron. 2014;52:196.
19. Kaur G, Saha S, Tomar M, Gupta V. Influence of immobilization strategies on biosensing response characteristics: a comparative study. Enzym Microb Technol. 2016;82:144.
20. Al-Ghamdi AA, Mahmoud WE, Yaghmour SJ, Al-Marzouki FM. Structure and optical properties of nanocrystalline NiO thin film synthesized by sol–gel spin-coating method. J Alloys Compd. 2009;486:9.

21. Reddy AM, Reddy AS, Reddy PS. Thickness dependent properties of nickel oxide thin films deposited by dc reactive magnetron sputtering. Vacuum. 2011;85:949.
22. Zhao ZW, Chen XJ, Tay BK, Chen JS, Han ZJ, Khor KA. A novel amperometric biosensor based on ZnO: Co nanoclusters for biosensing glucose. Biosens Bioelectron. 2007;23:135.
23. Stetsyshyn Y, Donchak V, Harhay K, Voronov S, Raczkowska J, Budkowski A. Modification of poly(ethylene terephthalate) surface with attached dextran macromolecules. Polym Int. 2009;58:1034.
24. Arora K, Tomar M, Gupta V. Highly sensitive and selective uric acid biosensor based on RF sputtered NiO thin film. Biosens Bioelectron. 2011;30:333.
25. Solanki PR, Kaushik A, Ansari AA, Malhotra BD. Nanostructured zinc oxide platform for cholesterol sensor. Appl Phys Lett. 2009;94:143901.
26. Aravamudhan S, Kumar A, Mohapatra S, Bhansali S. Sensitive estimation of total cholesterol in blood using Au nanowires based micro-fluidic platform. Biosens Bioelectron. 2007;22:2289.
27. Tang D, Yuan R, Chai Y, An H. Magnetic-core/porous-shell CoFe2O4/SiO2 composite nanoparticles as immobilized affinity supports for clinical immunoassays. Adv Funct Mater. 2007;17:976.
28. Liu S, Ju H. Reagentless glucose biosensor based on direct electron transfer of glucose oxidase immobilized on colloidal gold modified carbon paste electrode. Biosens Bioelectron. 2003;19:177.
29. Laviron E. Adsorption, autoinhibition and autocatalysis in polarography and in linear potential sweep voltammetry. J Electroanal Chem Interfacial Electrochem. 1974;52:355.
30. Guidelli R, Compton RG, Feliu JM, Gileadi E, Lipkowski J, Schmickler W, et al. Pure Appl Chem. 2014;86:245.
31. Khan R, Kaushik A, Solanki PR, Ansari AA, Pandey MK, Malhotra BD. Zinc oxide nanoparticles-chitosan composite film for cholesterol biosensor. Anal Chim Acta. 2008;616:207.
32. Laviron E. General expression of the linear potential sweep voltammogram in the case of diffusionless electrochemical systems. J Electroanal Chem Interfacial Electrochem. 1979;101:19.
33. Ansari AA, Kaushik A, Solanki PR, Malhotra BD. Electrochemical cholesterol sensor based on tin oxide-chitosan nanobiocomposite film. Electroanalysis. 2009;21:965.
34. Matharu Z, Solanki PR, Gupta V, Malhotra BD. Mediator free cholesterol biosensor based on self-assembled monolayer platform. Analyst. 2012;137:747.
35. Singh S, Chaubey A, Malhotra BD. Amperometric cholesterol biosensor based on immobilized cholesterol esterase and cholesterol oxidase on conducting polypyrrole films. Anal Chim Acta. 2004;502:229.
36. Umar A, Rahman MM, Vaseem M, Hahn YB. Ultra-sensitive cholesterol biosensor based on low-temperature grown ZnO nanoparticles. Electrochem Commun. 2009;11:118.
37. Szymanska I, Radecka H, Radecki J, Kaliszan R. Electrochemical impedance spectroscopy for study of amyloid β-peptide interactions with (−) nicotine ditartrate and (−) cotinine. Biosens Bioelectron. 2007;22:1955.
38. Gopalan AI, Lee KP, Ragupathy D. Development of a stable cholesterol biosensor based on multi-walled carbon nanotubes–gold nanoparticles composite covered with a layer of chitosan–room-temperature ionic liquid network. Biosens Bioelectron. 2009;24:2211.
39. Solanki PR, Kaushik A, Ansari AA, Tiwari A, Malhotra BD. Multi-walled carbon nanotubes/sol–gel-derived silica/chitosan nanobiocomposite for total cholesterol sensor. Sensors Actuators B. 2009;137:727.
40. Sharma R, Sinha RK, Agrawal VV. Electroactive Prussian blue encapsulated iron oxide nanostructures for mediator-free cholesterol estimation. Electroanalysis. 2014;26:1551.
41. Singh J, Srivastava M, Kalita P, Malhotra BD. A novel ternary NiFe 2 O 4/CuO/FeO-chitosan nanocomposite as a cholesterol biosensor. Process Biochem. 2012;47:2189.
42. Ali MA, Singh N, Srivastava S, Agrawal VV, John R, Onoda M, et al. Chitosan-modified carbon nanotubes-based platform for low-density lipoprotein detection. Appl Biochem Biotechnol. 2014;174:926.
43. Matharu Z, Sumana G, Solanki PR, Gupta V, Malhotra BD. Langmuir–Blodgett films of polyaniline for low density lipoprotein detection. Thin Solid Films. 2010;519:1110.